applied sciences

MDPI

Article

GIS-Based Optimal Route Selection of Submarine Cables Considering Potential Seismic Fault Zones

Nikolaos Makrakis [1], Prodromos N. Psarropoulos [2] and Yiannis Tsompanakis [1,*]

[1] School of Chemical and Environmental Engineering, Technical University of Crete, 73100 Chania, Greece
[2] School of Rural, Surveying and Geoinformatics Engineering, National Technical University of Athens, 15780 Athens, Greece
* Correspondence: jt@science.tuc.gr; Tel.: +30-28210-37634

Featured Application: As described in the examined case studies, the developed GIS-based computational tool can be efficiently applied for the selection of the optimal routing of energy and telecommunication cables by considering various design criteria and potential geohazards.

Abstract: Submarine lifelines (pipelines and cables) often cross areas characterized by earthquake-related geohazards (tectonic faulting, landslides and seabed liquefaction). Avoiding geologically hazardous areas increases the length (i.e., cost), whereas a potential crossing may detrimentally affect the structural performance of the infrastructure, requiring more sophisticated design approaches and/or more costly and probably impractical deep sea condition-mitigation measures. Under such adverse conditions, a cost-effective and resilient lifeline route is deemed necessary. The current paper presents a smart decision-support tool for the optimal route selection of submarine cables, assessing whether the proposed routing could effectively cross a (seismically) geologically hazardous area. The GIS-based tool is based on an efficient methodology that combines a least-cost path analysis with a multi-criteria decision method. Accordingly, several routes can be derived for user-defined scenarios, by assigning different weight factors in the adopted design criteria and hazards. When crossing fault zones, the problem of fault-cable intersection is quantitatively assessed in a realistic manner via advanced numerical models. The optimal route can be selected by considering the potential cable distress (i.e., exceedance of allowable cable strains). This tool can be efficiently implemented for deriving the optimal route of energy and telecommunication offshore cables, as it is described in the examined real case studies.

Keywords: telecommunication cables; power transmission cables; earthquake-triggered geohazards; fault rupture; fault-cable intersection; cable distress; optimal route selection; geographic information systems

Citation: Makrakis, N.; Psarropoulos, P.N.; Tsompanakis, Y. GIS-Based Optimal Route Selection of Submarine Cables Considering Potential Seismic Fault Zones. *Appl. Sci.* **2023**, *13*, 2995. https://doi.org/10.3390/app13052995

Academic Editor: Jong Wan Hu

Received: 2 February 2023
Revised: 22 February 2023
Accepted: 24 February 2023
Published: 26 February 2023

1. Introduction

The constantly increasing demands for energy and telecommunications worldwide have led to the continuous design, construction and operation of power transmission and telecommunication cables. Such critical lifelines (CLs) are expensive engineering projects that cover hundreds to thousands of kilometers, onshore and/or offshore, while their uninterrupted and safe operation is of paramount importance. On the one hand, submarine power cables, that have a relatively low environmental impact, can contribute to the rapid development of green energy sources, connecting offshore wind and solar farms to onshore power plants, as well as cross-border onshore energy stations [1]. On the other hand, offshore telecommunication cables play a key role in telecommunications and internet, as they can transmit data and information at high speeds around the world.

It is noteworthy that almost 99% of communications worldwide are performed through the existing 1.2 million kilometer network of submarine cables [2]. Time delays in transporting information through submarine telecommunication cables could lead to extreme

financial losses. Indicatively, Amazon has reported that every 100 milliseconds of delay could cost up to 1% of profits [2], while the Swiss Federal Institute of Technology has reported that a hypothetical one-week internet blackout in Switzerland could cost a monetary loss of over 1.2% of the country's GDP [3].

The strict environmental policies that have been established due to the intensification of environmental pollution and the increasing awareness for environmental protection, along with the over-increasing demands for cost-feasibility and resilient facilities that work safely and reliably during their lifetime, have necessitated the environmentally-friendly and techno-economically efficient design of CLs [2,4]. In parallel, using mitigation measures to prevent the potential failure of a submarine cable, especially in deep and ultra-deep waters, could be a rather limited and/or expensive solution; therefore highlighting the importance of routing optimization of such infrastructure. Although selecting the optimum route can considerably reduce the probability of failure and the life-cycle costs of the cable, it is usually dominated by a series of critical factors related to environmental, geopolitical, financial and technical aspects [2,5].

In engineering practice, the submarine cable route selection process, which is almost identical to the route selection of offshore pipelines, is manually carried out based on a very time-consuming procedure that relies on the engineering judgment and subjective opinion of the experts [6]. In brief, a suitable corridor is initially defined and graphically designed based on data (from charts, bathymetric contours, etc.) of the region under consideration. A preliminary survey is carried out along the specific corridor, several reasonable routes are designed, and after processing and evaluating the survey data and ensuring that all hazards or obstacles are completely avoided or eliminated, the optimum cable route is selected. Nevertheless, the application of several project-related advanced criteria, constraints, guidelines, etc., which increase the complexities of the route selection process, are not taken into account, and consequently, this heuristic approach cannot guarantee the optimal path.

To overcome this problem, mathematical models and algorithms, unaffected by human bias, have gradually been developed, aiming to facilitate the optimal route selection of CLs [3,7–9]. Nonetheless, in order to handle the enormous amount of data that are required to perform such complex spatial multi-criteria applications and effectively visualize the corresponding results, the advanced capabilities of geographic information systems (GIS) have been adopted. GIS constitute a powerful tool for multi-criteria analysis, since they provide the efficient methodology of the least-cost path analysis (LCPA). The LCPA, which was introduced in 1957 by Warntz [10], is usually applied to determine the optimal path between two points, and it can be additionally combined with advanced multi-criteria decision methods (MCDMs), such as the analytical hierarchy process (AHP). The integration of MCDM and GIS has been successfully applied for land-use [11] and site suitability analysis [12], urban planning and development problems [13,14], as well as for the route selection of CLs (e.g., [2,15,16]).

LCPA can handle several spatial criteria related to the effectiveness maximization and cost minimization of the CLs in a computationally efficient manner [17]. The selected criteria can be weighted in accordance with the requirements and constraints of the project (budget, accessibility, etc.). Several studies have reported the application of GIS in the optimal route selection of submarine CLs, reducing project costs by up to 30% [7,18–21]. In addition, it is worth noting that the route optimization of offshore large-scale engineering projects is suggested by international standards, such as the guidelines of the American Bureau of Shipping (ABS) [22].

Nonetheless, seismicity and the subsequent earthquake-triggered geohazards, such as slope instabilities, soil liquefaction and tectonic and non-tectonic faulting [23] (which have a high probability of occurrence during the lifetime of the infrastructure) constitute crucial factors during the process of optimal route selection, since they may have a remarkable impact on the structural performance of a CL [6,24]. These factors can be underestimated or improperly taken into account during the optimal route selection of CLs if they are treated

based only on engineering judgment. In particular, decisions related to disaster planning are often taken by the stakeholders, either manually or by utilizing the aforementioned mathematical models and/or the GIS-based techniques based on heuristics and rules of thumb [25]. Consequently, a route can be selected that either completely avoids all of the geologically hazardous areas or crosses them without adequately assessing the potential structural distress [26]. On the one hand, the complete avoidance of such areas constitutes an over-conservative approach, which might lead to economically unfeasible routings, as the length (and therefore the cost) of the CL may considerably increase. On the other hand, crossing geologically hazardous areas is a challenging issue that may detrimentally affect the integrity and functionality of the CL, while costly and impractical mitigation measures may be required.

Indicatively, many severe failures of submarine cables due to earthquake events and earthquake-related geohazards have been reported during the last decades. For instance, the earthquake-triggered geohazards due to the 6.8-magnitude Boumerdes earthquake, that occurred in Algeria in 2003, damaged at least six submarine fiber-optic cables, thus affecting the transmission of data and information throughout the Mediterranean region [24]. The 7.1-magnitude Pingtung earthquake in Southern Taiwan in 2006 caused an extensive internet and telecommunications disruption in South East Asia, as more than 20 offshore fiber-optic cables were broken or suffered severe damages [27]. The 2011 severe earthquake in East Japan affected a network of telecommunication cables of a total length greater than 2500 km [28].

Obviously, submarine cables are vulnerable to severe earthquakes and the resulting soil deformations due to earthquake-triggered geohazards. Considerable research effort has been concentrated on the cost-effective and resilient cable route selection considering earthquake hazard information and likelihood maps in conjunction with stochastic models for the occurrence of the earthquakes [5,29–31]. However, the problem of fault-cable intersection constitutes a challenging topic that has not been thoroughly investigated, thus, few relevant publications can be found in the literature. Wang et al. [32] conducted a full-scale experiment and performed a comprehensive parametric study to numerically investigate the problem of fault-cable intersection in the case of strike-slip faults, considering quasi-static loading conditions. Cao et al. 2016 [33] examined the problem of fault-cable intersection utilizing an analytical optimization approach considering, as objectives, both cost and cable breaking probability. In contrast, significant experimental [34–36], numerical [37–39] and analytical [40–42] research has been conducted to address the problem of faut-pipeline intersection.

Therefore, further research is required for the seismic design and optimal route selection of submarine cables, assessing whether the proposed routing could effectively cross a (seismically) geologically hazardous area by quantifying the criticality of the potential problems (i.e., exceedance of allowable strains of the cable). Recently, the authors facilitated the optimal route selection of large-scale engineering projects (such as natural gas pipelines) subjected to earthquake-triggered geohazards (i.e., seismic fault rupture and submarine slope instability) through the development of a GIS-based smart decision-support tool [26,43]. The structural performance of the pipeline was evaluated through finite-element analyses and (semi-)analytical models and the corresponding results were combined, in the form of an advanced criterion, with the LCPA technique within the GIS environment.

The current work presents an upgraded version of the aforementioned smart tool, which aims to achieve the optimal route of submarine fiber-optic and power transmission cables, taking into account—among other criteria—the quantitative assessment of the geohazard of fault rupture and the consequent cable distress. The main novelty of the developed smart tool is that it efficiently combines different software (i.e., for the geospatial process of optimal route selection and for the numerical analysis of the cables), supporting tools (i.e., Python scripts) and decision-making methodologies (MCDM). More specifically, the GIS-based LCPA technique is successfully combined with AHP to efficiently exploit

all possible routing alternatives of submarine cables in seismically geologically hazardous regions, such as the wider Mediterranean region. In particular, various scenarios have been considered by assigning different weight values to the adopted design criteria which include active fault zones. In addition, a different rating score has been assigned to each fault zone in order to assess more realistically their potential impact on the examined cables as much as possible. Analogous ratings are given to the other design criteria, i.e., seabed inclination and bathymetry.

It is noted that in previous studies, where AHP was combined with GIS for the route selection of CLs, earthquake-related geohazards, such as fault ruptures, were either completely ignored [2,16], or treated as absolute barriers (i.e., could not be crossed) without assessing the structural distress of a crossing CL. Consequently, their weight values were exemplified by defining them as "∞" [15]. This deficiency is alleviated in the current study, as efficient finite element (FE) numerical models for both energy and telecommunication submarine cables have been developed and have been integrated in the proposed GIS-based decision tool to realistically address the problem of fault-cable intersection. These FE models constitute another valuable contribution of the present work, as to the best of the authors' knowledge, there are only a very few relevant studies addressing this very important and demanding problem of offshore cable intersection with tectonic faults.

The applicability of the smart tool is verified via its implementation in three real case studies (i.e., an offshore telecommunication (fiber-optic) cable and two power transmission cables) in the southeastern Mediterranean Sea. Several scenarios are examined to illustrate the impact of assigning different weighting factors in the examined design criteria. Energy and telecommunication companies and operators can benefit from the proposed GIS-based computational tool, as it can be efficiently implemented in the optimal routing of submarine cables by considering various design criteria and potential geohazards.

The rest of the paper is organized as follows: Section 2 contains a step-by-step description of the developed decision-support tool. Section 3 initially describes the area under consideration and subsequently, presents the examined case studies and the alternative cable routes obtained from the application of the smart tool. Section 4 discusses the derived routes and the results from the numerical analyses. Finally, Section 5 presents the main findings of the study, the advantages and disadvantages of the proposed smart decision-support tool and the adopted methodologies.

2. Materials and Methods

The newly-developed smart decision-support tool has been built in the ArcGIS Desktop GIS computational platform, utilizing the ArcMap GIS software [44]. Nevertheless, other ArcGIS software, such as ArcGIS Pro, could also be used with the same effectiveness. In its present version, the GIS-based LCPA technique has been automatically combined with the AHP methodology and (semi-) automatically with the finite element models that have been developed by the authors via suitable scripts that have been developed utilizing Python programming language. More specifically, the optimal route of an offshore cable is selected, taking into account, among others, the quantitative assessment of the structural behavior of the cable subjected to the seismic geohazard of tectonic faulting.

Initially, all available geodata related to the topography, geology, bathymetry, seismicity and geotectonics of the examined area were collected and stored in an extensive geodatabase within the GIS environment, as separate thematic layers. Following suitable data processing, each thematic layer was converted into a basic criterion for the AHP method and subsequently, for the LCPA technique. Having defined the basic criteria, AHP was applied and the qualitative prioritization of the criteria was transformed into weight values. Then, the GIS-based LCPA technique was applied, and several length- and cost-minimized cable routes were derived, corresponding to the different user-defined scenarios.

Whenever the derived cable routings crossed seismically active fault zones, numerical analyses were performed to quantitatively assess the problem of fault-cable intersection, by assessing the structural distress of the cable in terms of strains. Finally, provided that

the strains of the cable were below the acceptable limits, the optimal route was selected, else the process was repeated to derive alternative routings. Figure 1 depicts the main steps of the current version of the smart tool, whereas a detailed description of each step is provided in the sequence.

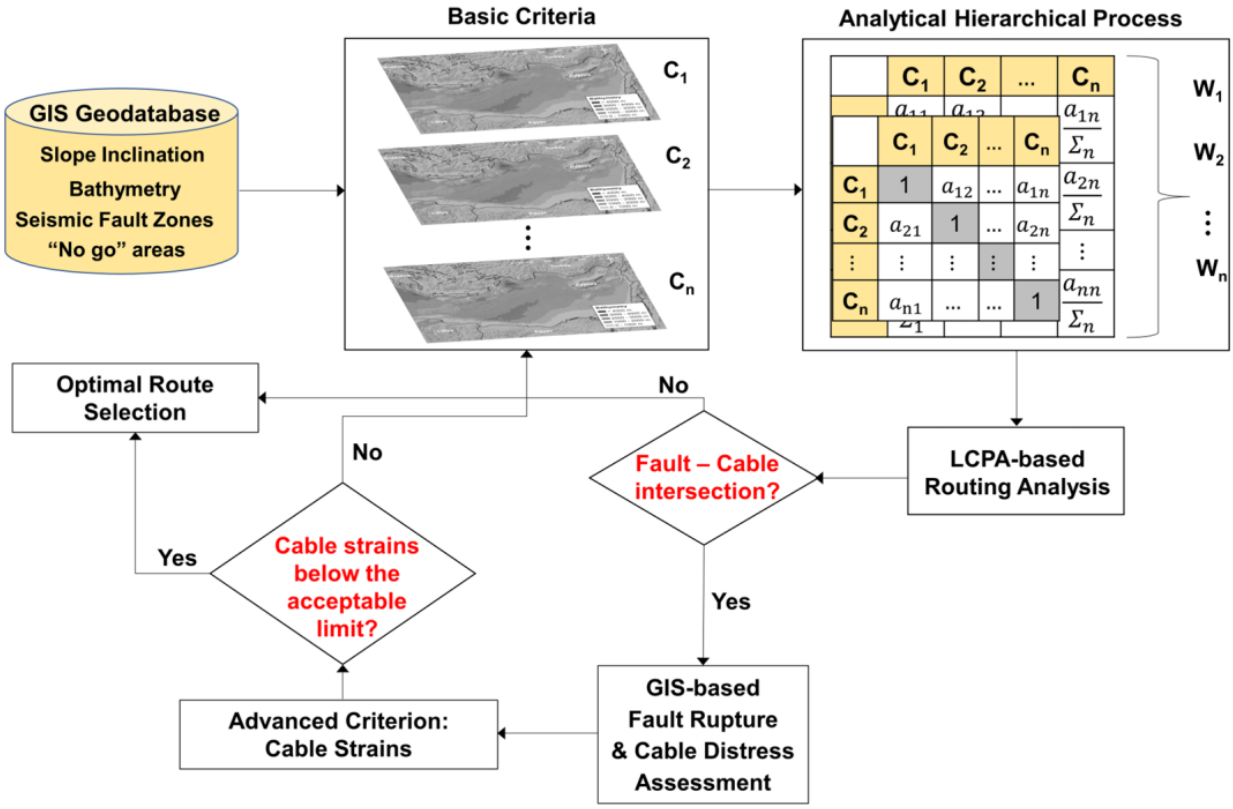

Figure 1. Flowchart of the developed smart decision-support tool.

2.1. GIS Geodatabase and Basic Criteria

Creating the GIS geodatabase, collecting and organizing the required spatial geodata constitute very important steps during the process of optimal route selection, since stakeholders and experts can then obtain a digital and detailed general aspect of the area under consideration. The created GIS database contains spatial geodata in the form of shapefiles and GeoTIFF. In case of insufficient digital data, existing maps are scanned/digitized and added in the GIS environment. Depending on the information they contain, geodata are organized into different thematic layers, which are subsequently utilized as basic criteria for the routing analysis.

Generally, geodata are distinguished into vector (i.e., points, lines and polygons (areas)) and raster (matrices of pixels (i.e., cells) with rows and columns) [44]. However, since the LCPA technique requires data that change continuously across a landscape (i.e., cost surface), all of the vector geodata are further processed and converted into raster. To increase the accuracy and reliability of the developed smart tool, all of the selected geodata are reclassified to the same number of classes and resampled to have the same spatial resolution [45].

Since optimal route selection is a complex multi-criteria procedure, several criteria are usually taken into account in real case studies, such as areas where cable alignment is a priori prohibited (e.g., military and unexploded ordnance (UXO) areas, marine parks and NATURA 2000 areas, as well as wrecks and anchorage locations) and dangerous zones, including seabed slopes with large inclination, areas of intense seismicity, geology, etc. [26].

2.2. Analytical Hierarchical Process

A complex decision-making system consists of several sub-factors (i.e., criteria) that have to be comprehensively weighted according to their importance in the system. Nevertheless, determining the weight values constitutes a challenging task, since it is usually influenced by the experience and the knowledge of the experts [46]. For this reason, unbiased multi-criteria decision methodologies have been gradually developed. The rationality of weight distribution has been improved, since the aforementioned methodologies are based on scientific procedures that efficiently decompose complex decision-making systems into sub-factors. These sub-factors are stratified by a dominance relationship, which results in the desired weight values after a pairwise comparison. The analytic hierarchy process (AHP), which was introduced by Saaty in the 1970s [47], constitutes a consistent multi-criteria methodology that is based on decision-making theory and has been proven very effective in a wide variety of real case studies that involve several interrelated objectives [48].

When utilizing AHP, the criteria of the project are identified, and a $n \times n$ criteria comparison matrix A is constructed as follows:

$$[A] = [a_{ij}] = \begin{array}{c|cccc} & C_1 & C_2 & \dots & C_n \\ C_1 & 1 & \alpha_{12} & \dots & \alpha_{1n} \\ C_2 & \alpha_{21} & 1 & \dots & \alpha_{2n} \\ \vdots & \vdots & \vdots & \vdots & \vdots \\ C_n & \alpha_{n1} & \dots & \dots & 1 \end{array} \qquad i, j = 1,2,3 \dots, n \tag{1}$$

where C_i ($i = 1, 2, 3 \dots, n$) are the adopted criteria (corresponding to matrix rows and columns, indicatively shown in the shaded areas), n is the number of criteria and α_{ij} denotes a ranking score assigned to each criterion in terms of its importance, using an evaluation scale from $1/9$ to 9. It is noted that the values of α_{ij} and its transpose α_{ji} are inversely proportional, i.e., $\alpha_{ji} = 1/\alpha_{ij}$. A score equal to $1/9$ indicates that the criterion in the column is much more important than the criterion in the row of matrix A, whereas when it is equal to 9, it implies the opposite. A value equal to 1 indicates the same importance for the two criteria [49] and it appears along the diagonal of A, since it corresponds to the pairwise comparison of the same criterion.

Accordingly, a pairwise comparison of each one of the selected criteria is carried out [50]. The rankings in every column of the A matrix are summed up and subsequently, each element of A is divided by the sum of the specific column, thus forming the normalized criteria comparison matrix $\overline{A}$ as follows:

$$[\bar{A}] = \left[\frac{a_{ij}}{\Sigma_k}\right] = \begin{array}{c|cccc} & C_1 & C_2 & \dots & C_n \\ C_1 & \frac{a_{11}}{\Sigma_1} & \frac{a_{12}}{\Sigma_2} & \dots & \frac{a_{1n}}{\Sigma_n} \\ C_2 & \frac{a_{21}}{\Sigma_1} & \frac{a_{22}}{\Sigma_2} & \dots & \frac{a_{2n}}{\Sigma_n} \\ \vdots & \vdots & \vdots & \vdots & \vdots \\ C_n & \frac{a_{n1}}{\Sigma_1} & \dots & \dots & \frac{a_{nn}}{\Sigma_n} \end{array} \qquad i, j = 1,2,3 \dots, n. \tag{2}$$

where, $\Sigma_k = a_{1j} + a_{2j} + \dots + a_{nj}$ for each column $j = 1, 2, 3 \dots, n$. Having set up $\overline{A}$, the average of each row is calculated as shown in Equation (3), and the weights are derived for each criterion to form priority vector W:

$$\{W\} = \overline{W_i} = \sum_{j=1}^{n} \overline{a_{ij}} \qquad i, j = 1, 2, 3 \dots, n. \tag{3}$$

It is noted that W determines which of the adopted criteria is the most dominant for the design process.

A fundamental aspect of AHP is to ensure that the assigned evaluation factors are consistent. Hence, the numerical measures, namely the consistency index (CI) and consistency ratio (CR), have been established, aiming to guarantee the existence of the transitive property of matrix A, i.e., if criterion X is more important than Υ, and Υ is more important than Z, then X should be more important than Z. Initially, vector W_s is defined as the product of A and W, and subsequently, consistency vector C_v is derived by dividing each cell value of the matrix multiplication result vector by the corresponding priority vector cell as follows:

$$\{W_s\} = [A]\{W\} \tag{4}$$

$$\{C_v\} = \{W_s\}\left\{\frac{1}{W}\right\} \tag{5}$$

The eigenvalue of the algebraic system λ is obtained from the average of the elements of consistency vector C_v and it is utilized to calculate the value of CI. Moreover, the CR is calculated as:

$$CR = \frac{CI}{RI} \tag{6}$$

where RI denotes the random index, which represents the CR of a randomly generated matrix and its value depends on the number of criteria. RI can be derived from related publications [47]. Finally, if the resulted CR is lower than 0.1, the pairwise comparison matrix is consistent, which means that there are no pair combinations that would be unreasonable [51].

The authors have taken advantage of the advanced capabilities and high functionality of GIS to develop customized tools that are suitable for the needs of the examined applications using the Python site package for analysis and data management, ArcPy. Accordingly, a Python script has been programmed in order to successfully integrate the aforementioned matrices and relationships of AHP into the developed GIS model.

2.3. LCPA-Based Routing Analysis

Having defined the basic design considerations (i.e., basic criteria) and their quantitative prioritization (i.e., weight values), a preliminary multi-criteria routing analysis is conducted, implementing the LCPA technique. The latter constitutes a powerful and computationally efficient routing analysis methodology that has been broadly utilized for finding the shortest (and most cost-effective) path over a cost surface (i.e., raster surface) from a starting point to an ending point. GIS-driven LCPA is based on a variant of the Dijkstra's algorithm [52]. The latter has been widely used to process the optimal route selection of cables [2,5]. In contrast to other similar techniques, LCPA guarantees the solution of the shortest path problem, as all possible nodes within the entire cost surface are examined, all of the suitable "corridors" (i.e., paths) are identified and consequently, the most cost-effective one between the two geographic points is determined [44,53,54].

Initially, all of the origin's neighboring cells are checked along the horizontal, vertical and diagonal directions, and the one that contains the lowest cost value is identified. Subsequently, the cell with the lowest value is converted into the starting point and the next cell with the lowest value is identified. Through an iterative procedure, the user-defined origin and destination points are eventually connected. Then, the already-found cells with the lowest cost value are utilized in a back-propagation process from the destination to the origin point and the desired least-cost path is finally derived [55,56]. In the ArcMap commercial GIS software package, LCPA is carried out through the serial application of GIS spatial analyst tools [26,43].

Lastly, it is important to clarify that the routing analysis can be undertaken multiple times depending on the number of different scenarios that have to be examined (i.e., all time different weighted factors are assigned to the considered criteria) according to the user's preferences, and consequently, several alternative routings are derived.

2.4. GIS-Based Fault Rupture and Cable Distress Assessment

2.4.1. Numerical Modeling of Cable Distress

The structural performance of the cable due to offshore fault-cable intersection has been simulated employing the static standard module of the ABAQUS finite element (FE) software [57]. Beam elements have been used to represent the cable, whereas the cable-soil interaction has been simulated by means of pipe-soil interaction (PSI) elements along the axial and vertical directions. PSI elements usually lead to more accurate and realistic results compared to the conventional soil springs. The two nodes of PSI elements are attached to the cable, while the other two represent the soil, thus facilitating the assessment of soil resistance.

A cable of typically infinite length has been taken into consideration to minimize the effect of undesired boundary conditions at the edges of the FE model. The fault movement is imposed on the one end of the cable and the corresponding far-field PSI nodes, whereas the other end of the cable and the PSI nodes are fixed. Figure 2 depicts the employed FE modeling of the cable. It is noted that only the case where the rupture bedrock is not covered from soft seabed sediments has been simulated herein. The impact of the presence of soft sediments on fault rupture propagation and the corresponding distress of offshore CLs has been numerically examined by the authors' group [58].

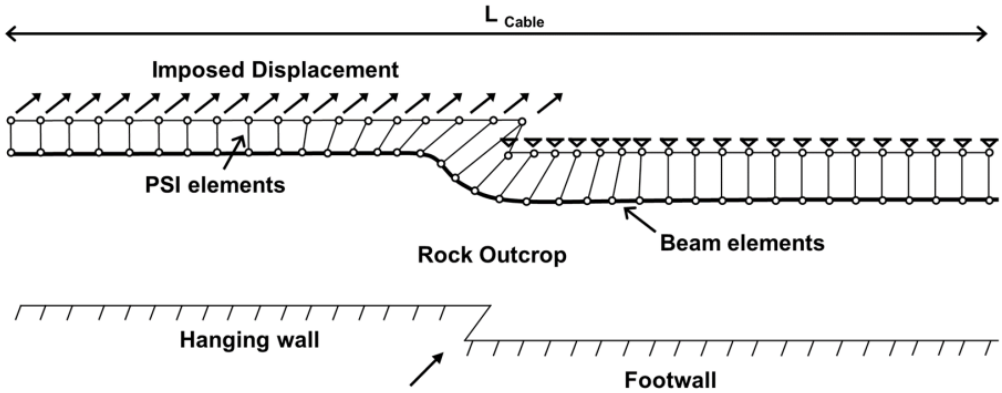

Figure 2. Proposed numerical model for cable-fault intersection.

2.4.2. Verification against the Experimental Results

The validity of the proposed numerical model has been verified with the results from a full-scale experiment that was carried out by Wang et al. [32]. A large-scale split-box test apparatus with dimensions of 5 m × 1 m × 1 m (length × width × height) was filled with dry sand with an average particle size of D_{50} = 0.553 mm and unit weight of γ = 17.4 kN/m^3, whereas the peak and critical state friction angles were set equal to 47.7° and 33.5°, respectively. A 5 m-long light weight (LW) cable of nominal outer and inner diameters equal to 18 mm and 1.9 mm, respectively, and elastic modulus, E = 22.8 GPa, was buried 0.5 m within the soil.

To reliably simulate the anchored conditions, which usually occur at the seabed, both ends of the cable were fixed. The cable was subjected to abrupt lateral ground movements, which were physically simulated by keeping fixed the one half of the apparatus box and moving the other half along its longitudinal axis. A horizontal displacement was quasi-statically imposed (i.e., on a ratio approximately equal to 2 mm/min) almost up to the displacement capacity of the test apparatus (i.e., 300 mm), and the structural response of the cable, in terms of strains, was evaluated utilizing strain gauges.

Submarine telecommunication and power cables are characterized by complex and multilayered cross-sectional configurations and their mechanical behavior is not easily attainable. As a consequence, the numerical simulation of such CLs constitutes a challenging task and numerous assumptions and simplifications are usually required [32,59,60]. Wang et al. [32] numerically verified their experimental results and addressed the aforementioned structural complexities by adopting an equivalent cross-section of an LW telecom-

munication cable consisting of a unique material with equivalent tensile strength and elastic modulus, as shown in Figure 3. More specifically, the equivalent cross-section had the same outer and inner diameter, i.e., 18 mm and 1.9 mm, respectively, whereas the equivalent elastic modulus was defined as the ratio of the tensile strength to the equivalent cross-sectional area and it was estimated to be equal to 30 GPa.

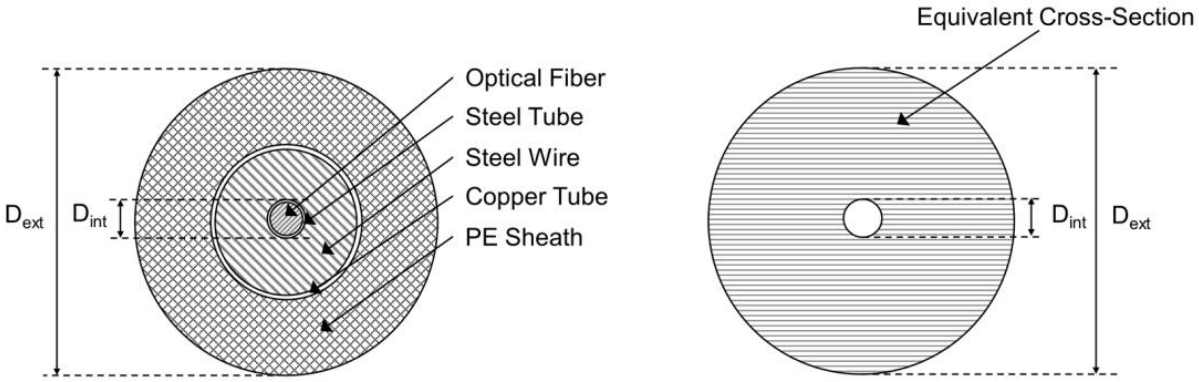

Figure 3. LW submarine cable and its equivalent cross-section.

Having defined the geometry and mechanical properties of the equivalent cross-section, Wang et al. [32] utilized beam elements to model the cable, whereas the cable-soil interaction was simulated using PSI elements along the axial and transverse horizontal directions. One node of each PSI was attached to the cable, while the soil displacement was imposed on the far-field node of the PSI. Five lateral soil displacements ranging from 50 mm to 200 mm were taken into account and the structural response of the cable was plotted in terms of axial, bending and total strains along its length. The obtained results revealed a good agreement with the experimental results, as shown in Figure 4.

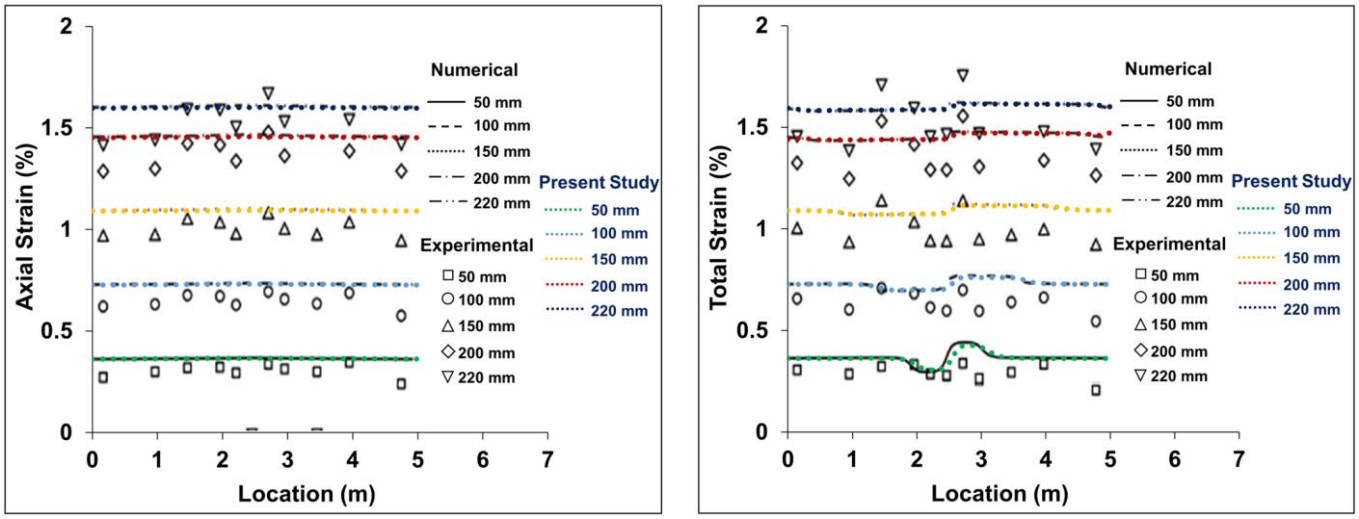

(**a**) (**b**)

Figure 4. Comparison of the proposed FE model and the experimental and FE model of Wang et al. [32] for the response of a submarine cable to the lateral seabed movement in terms of: (**a**) axial strains and (**b**) total strains.

In the current study, a simple numerical model has been initially developed, based on the details given by Wang et al. [32]. Figure 4 demonstrates the very good agreement of the developed FE model results with the experimental and the numerical results of the previous study. Following the successful verification of the adopted numerical methodology, more

elaborate models have been developed to simulate the realistic cases of submarine cables with much different cable geometry and material properties, as well as faulting conditions.

It is stressed that due to a lack of studies investigating the problem of fault-power cable intersection, an equivalent cross-sectional configuration has been adopted for the numerical modeling of the submarine power transmission cable, as shown in Figure 5. The original cross-section of the power cable has been adopted from Fang et al. [59]. It is highlighted that the circular solid beam elements (i.e., without internal diameter) have been utilized, compared to the cross-section that has been used for the numerical modeling of the telecommunication cable. This is attributed to the fact that optical fibers (which are located in the middle of the cross-section, as shown in Figure 3) are usually made of glass and as a consequence, they do not exhibit permanent deformations. Moreover, a conductor made from steel is usually located in the middle of the cross-sectional configuration of power transmission cables.

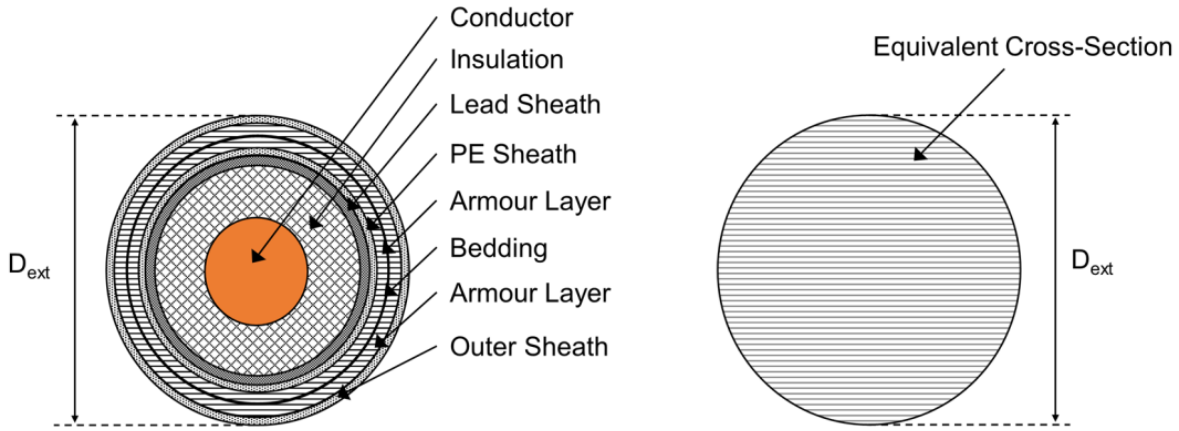

Figure 5. Submarine power cable and its equivalent cross-section.

2.5. Optimal Route Selection

The advanced capabilities of GIS that enable the use of Python programming language, through the Python site package for analysis and data management, ArcPy, or Visual Basic for Applications (VBA), have been utilized to combine the developed GIS model with the results obtained from the numerical analyses. In particular, a Python script is created to automatically export the results from the output database of the ABAQUS FE software, in terms of absolute axial cable strains. The maximum value of the axial strain is computed utilizing a Python function in the aforementioned script. The script is embedded into the GIS model, while the absolute maximum axial strain is compared with the allowable cable strain via a simple if statement that is included in the script. If the resulting cable distress is lower than the indicative limit, the route can be selected as the optimal one for the specific criteria/weights of the AHP. Conversely, if the cable strain is greater than the limit, different scenarios are examined and the process of the smart decision support tool is iteratively performed, as shown in the flowchart of Figure 1. It is important to note that the interaction between two different software (i.e., GIS and ABAQUS) constitutes a challenging topic that is under constant development.

3. Results

The current version of the developed smart decision-support tool has been efficiently applied in the southeastern Mediterranean Sea. The main aim of the presented implementation is to optimize the routing of three real engineering projects, a submarine telecommunication cable connecting the island of Crete, Greece, with Libya, and two offshore power transmission cables that will be used in the near future to transfer energy to/from the island of Crete to Cyprus and Egypt, respectively.

Figure 6 provides a further insight of the area under consideration. For the realistic description of the seabed, a digital bathymetry model (DBM) has been created in the GIS

environment based on a GeoTIFF format file that was downloaded from OpenTopography.org [61]. The boundaries of the wider area of interest have been downloaded as a shapefile from Marineregions.org [62] and they have been further processed in GIS. The points represent the origin and destination points (i.e., their approximate locations at the coastline) of the examined case studies.

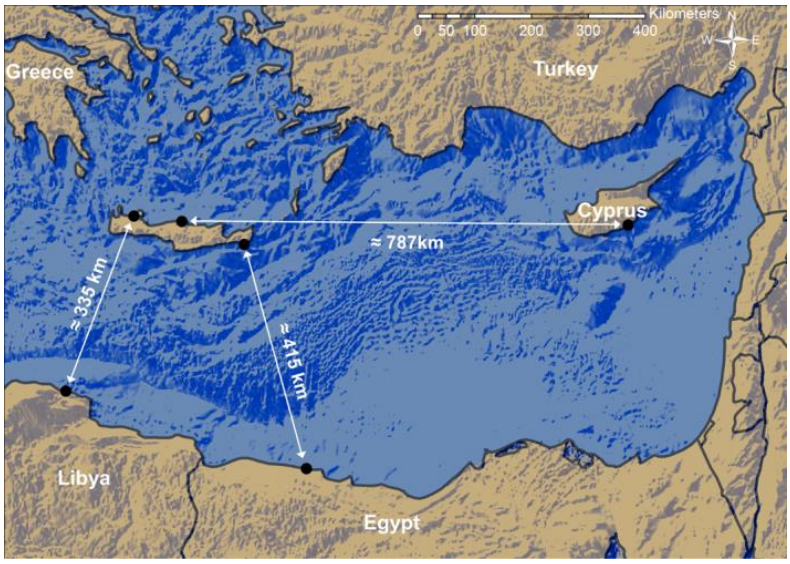

Figure 6. General view of the area under consideration.

Figure 7a–d depict all of the geodata that have been collected and further processed within the GIS environment. The data provided from the Shuttle Radar Topography Mission plus (SRTM plus) of a 30-arc second resolution global bathymetry grid have been utilized to represent the bathymetry of the area under consideration [63]. It is noted that for reasons of simplification, the bathymetric data herein (i.e., Figure 7a) are presented in the form of nested polygons for each depth (i.e., −200 m, −1000 m, −2000 m, −3000 m and −4000 m). The map in Figure 7b illustrates the seabed slope inclination, as derived from the GIS software. Seabed slope inclination varies from 0° to slightly more than 50°. Figure 7c depicts that numerous earthquake events of magnitude M $\geq$ 4.5 occurred between 1960 and 2022, especially near the island of Crete, according to the United States Geological Survey (USGS) [64].

According to Figure 7d, there are six main fault zones, four of them are located between the island of Crete and Libya: (i) the Cretan–Rhodes Ridge, (ii) the Hellenic trench, (iii) the East Mediterranean ridge and (iv) the Herodotus trough, whereas the remaining are observed near Cyprus: (v) the West Cyprus arc and (vi) the South Cyprus Trench. The aforementioned seismic fault zones have been acquired in the form of linear entities from a geospatial database infrastructure provided by the International Hydrographic Organization's Data Center for Digital Bathymetry (IHO DCDB) co-located with NOAA's National Centers for Environmental Information (NCEI) and maintained for the General Bathymetric Chart of the Oceans (GEBCO), under the auspices of the IHO and the UNESCO Intergovernmental Oceanographic Commission (IOC) [65] and the global database maintained by the Global Earthquake Model Foundation [66]. It is important to mention that the exact details regarding the geometry, the type and the potential maximum slip of the seismic fault zones are not available. In addition, Figure 8 presents a map showing the thickness of the sediments in the Mediterranean Sea, which was developed by Gennesseaux and Winnock [67] and is available at the International Hydrographic Organization Data Center for Digital Bathymetry (IHO-DCDB) in the framework of Seabed 2030 Project.

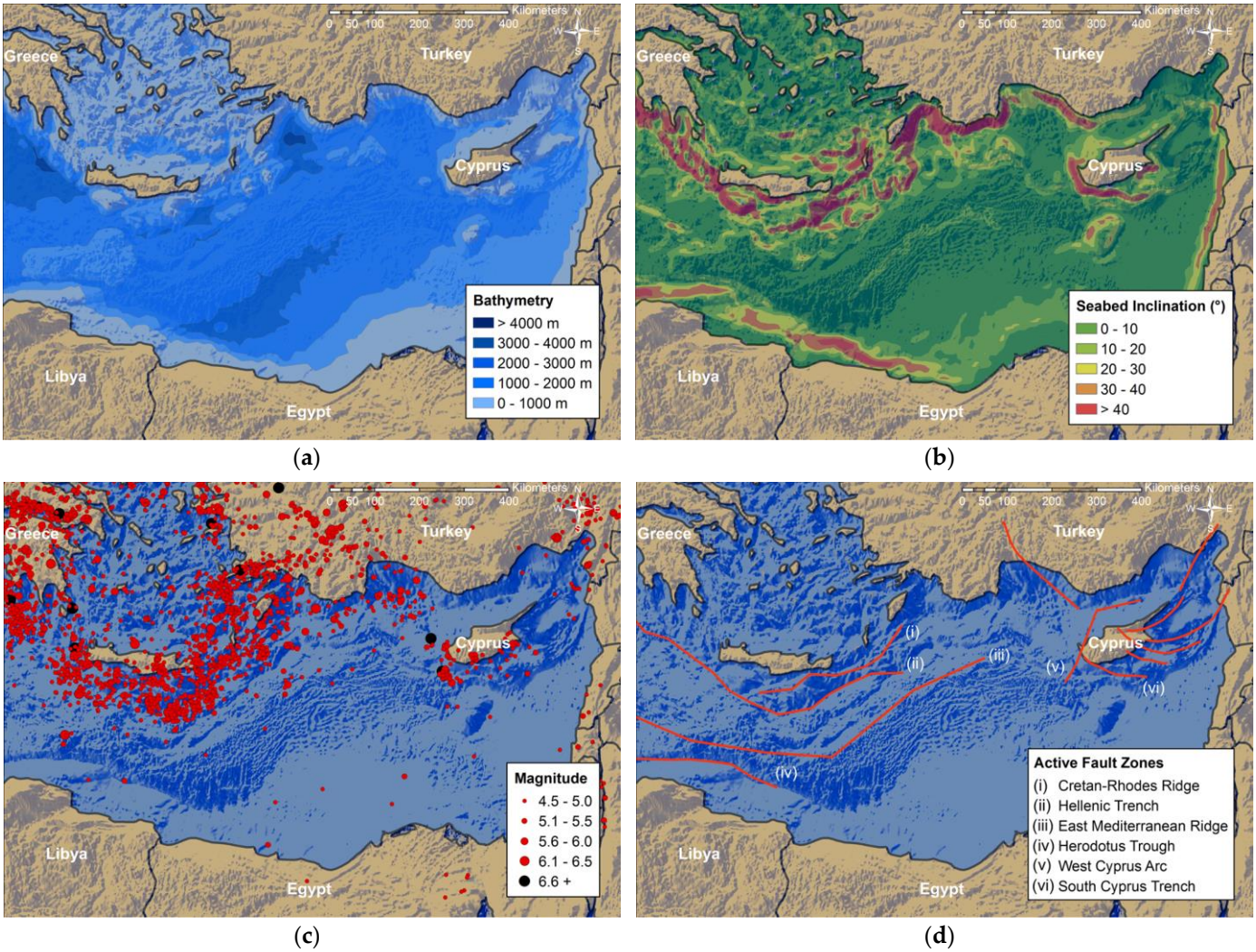

Figure 7. Geodata of the area under consideration for the application of the smart decision-support tool: (**a**) bathymetry, (**b**) seabed inclination, (**c**) seismicity and (**d**) major seismically active fault zones.

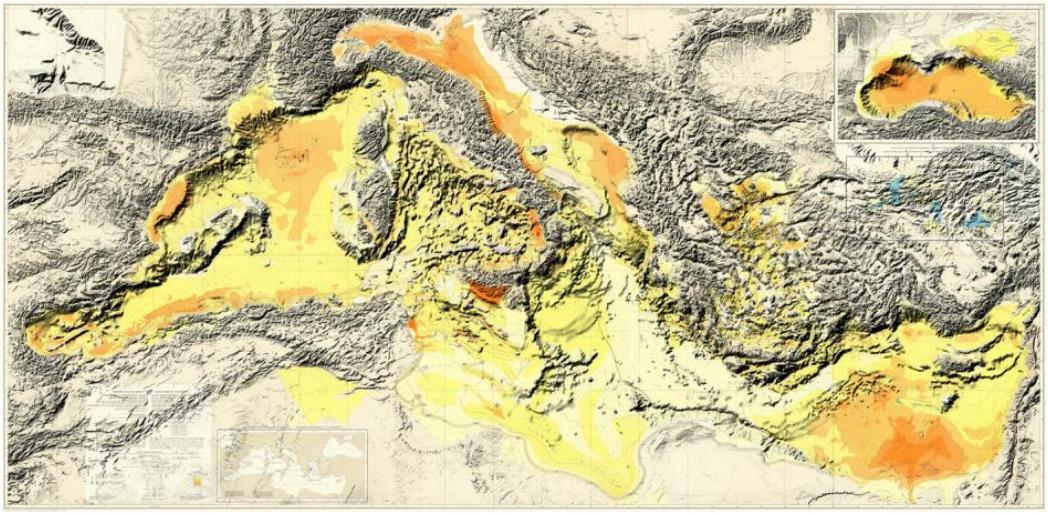

Figure 8. The thickness of the sediments on the seabed of the Mediterranean Sea (adopted from (https://www.ngdc.noaa.gov/mgg/ibcm/ibcmsedt.html (accessed on 1 February 2023)) [67]).

3.1. Validation of the Smart Decision-Support Tool

The reliability and effectiveness of the developed smart decision-support tool have been verified against a real engineering project, namely the EuroAsia Interconnector, which will be constructed in the near future. More specifically, a 1208 km long HVDC offshore cable is expected to transmit electricity between Israel, Cyprus and Greece. Herein, the optimal routing capabilities of the smart decision-support tool have been verified against the approximately 875 km long offshore cable (i.e., not considering the coastal and onshore parts) that will connect the island of Crete to Cyprus [68].

In complex multi-criteria analyses, each of the adopted criteria is usually distinguished into categories or sub-criteria. Herein, the spatially distributed criterion of seabed inclination has been reclassified into five classes (sub-criteria). Moreover, a rating score ranging from 1 to 5 has been applied to all of the adopted criteria, where 5 denotes a class that has to be avoided during routing analysis and 1 represents a class that a CL could cross. Table 1 summarizes the selected criteria, their weight values, as well as the sub-criteria and their rating score for the verification case study. Figure 9 shows the proposed route that has been derived from the application of the smart decision-support tool, and the designed route of the EuroAsia Interconnector.

Table 1. Weight-influence and rating score of each of the adopted criteria and sub-criteria.

Criteria	Weight-Influence (%)	Sub-Criteria	Rating Score
Seabed Inclination (°)	45	0–10	1
		10–20	2
		20–30	2
		30–40	3
		>40	3
Seismic Fault Zones	55	Cretan–Rhodes ridge	3
		Hellenic trench	5
		East Mediterranean ridge	2
		Herodotus trough	-
		West Cyprus arc	5
		South Cyprus trench	5

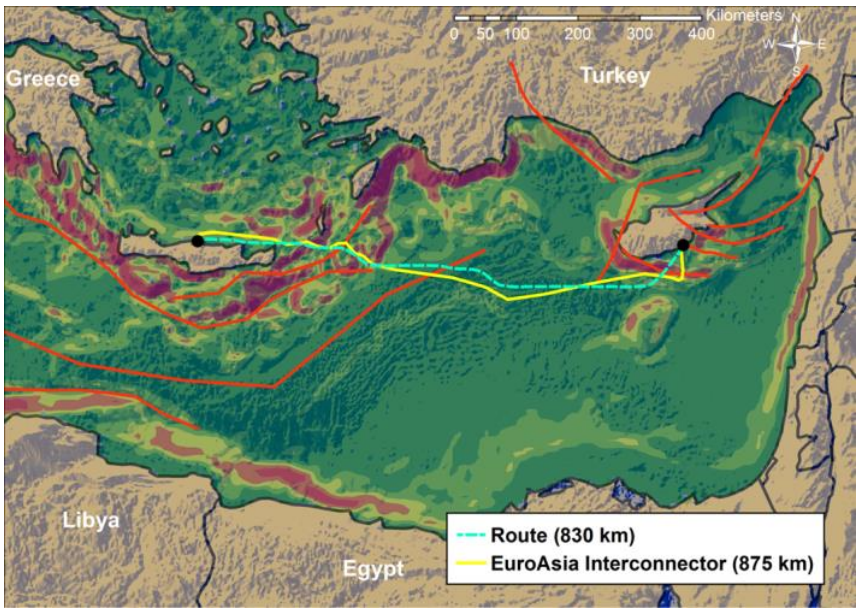

Figure 9. Verification of the routing analysis of the smart decision-support tool.

3.2. Case Study 1: Submarine Telecommunication Cable Connecting Crete with Libya

In the sequence, the smart tool has been applied to investigate several alternative routings in the case of a telecommunication cable, based on an existing routing of a cable connecting Crete with Libya. Seabed inclination, bathymetry and the seismically active fault zones have been taken into account as basic criteria for this case study. It should be noted that the presence of "no-go" areas has been neglected due to a lack of relevant data. The developed decision-support tool has been applied by examining the following five scenarios:

- Scenario 1

Seabed inclination is extremely more important than bathymetry and seismic fault zones, whereas bathymetry and seismic fault zones have the same importance.

- Scenario 2

Bathymetry is extremely more important than seabed inclination and seismic fault zones, whereas seabed inclination and seismic fault zones have the same importance.

- Scenario 3

Seismic fault zones are extremely more important than seabed inclination and bathymetry, whereas seabed inclination and bathymetry zones have the same importance.

- Scenario 4

An intermediate scenario where seabed inclination, bathymetry and seismic fault zones are equally important.

- Scenario 5

A realistic scenario where the qualitative prioritization of the criteria is based on the experience of cable routing engineers obtained from several industry partners. The utilized scale factors, which are summarized in Table 2, are in accordance with the study of Wang et al. [2].

Table 2. Qualitative prioritization for Case Study 1 with a consistency ratio equal to 0.0013.

	Seabed Inclination	**Bathymetry**	**Seismic Fault Zones**
Seabed Inclination	1	4	1/2
Bathymetry	1/4	1	1/9
Seismic Fault Zones	2	9	1

Table 3 presents the weight values that resulted from the AHP for each of the aforementioned scenarios, as well as the rating score for each sub-criterion. It is noted that similarly to seabed inclination, bathymetry has been distinguished into five sub-criteria.

Having assigned the weights and the rating score to the selected criteria, the LCPA technique has been applied within the GIS environment and five different cost (and length) minimized cable routes have been derived (i.e., five different scenarios). Figure 10a,b present the results of the routing analysis. In particular, Route I corresponds to the realistic scenario 5, Route II represents the extreme scenario 1, Route III denotes the extreme scenario with a greater weight value to seismic fault zones, Route IV constitutes the intermediate scenario, whereas Route V corresponds to the extreme scenario 2. In addition, the existing submarine telecommunication cable has been added for comparison.

The previously described numerical methodology has been applied to numerically simulate the problem of fault-cable intersection. A single armored (SA) submarine telecommunication cable of typically infinite length has been considered. An equivalent simplified cross-section has been developed, as shown in Figure 11. The outer diameter, D_{ext} has been set equal to 28 mm, whereas the inner diameter, D_{int} is equal to 1.9 mm. The equivalent elastic modulus has been set equal to 63.06 GPa according to Wang et al. [32].

Table 3. Weight-influence and rating score of each of the adopted criteria and sub-criteria for Case Study 1.

Criteria	Weight-Influence (%)					Sub-Criteria	Rating Score
	Scenarios						
	1	2	3	4	5		
Seabed Inclination (°)	82	9	9	33	30	0–10 10–20 20–30 30–40 >40	1 2 3 4 5
Bathymetry (m)	9	82	9	33	7	0–1000 1000–2000 2000–3000 3000–4000 >4000	1 2 3 4 5
Seismic Fault Zones	9	9	82	34	63	Cretan–Rhodes ridge Hellenic trench East Mediterranean ridge Herodotus trough West Cyprus arc South Cyprus trench	- 5 3 5 - -

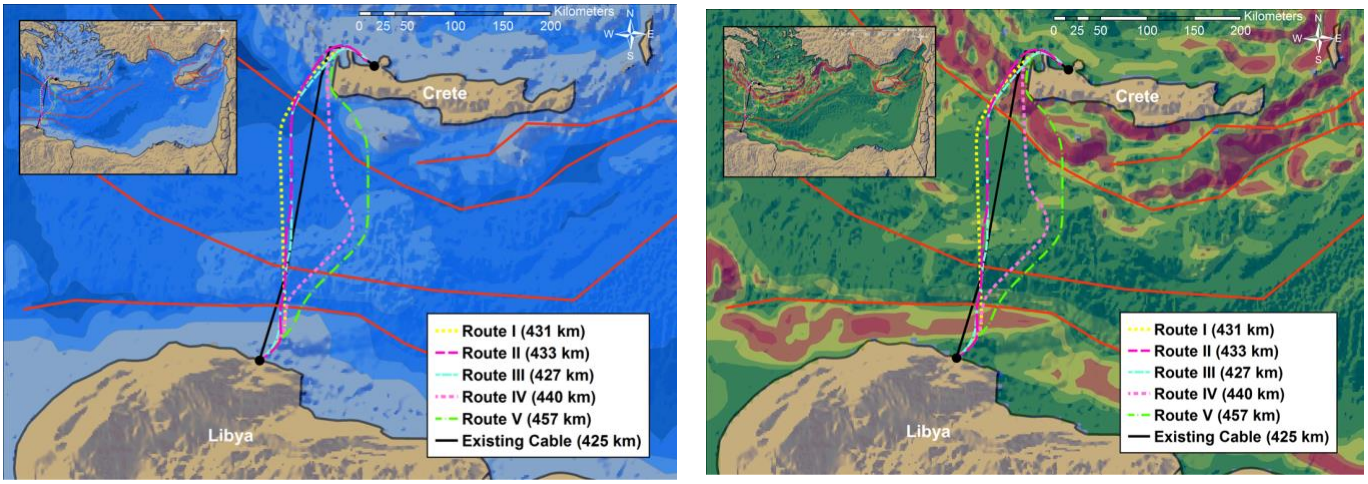

(**a**) (**b**)

Figure 10. Proposed alternative routes and seismically active fault zones: (**a**) with the bathymetry as a background and (**b**) with the seabed inclination as a background.

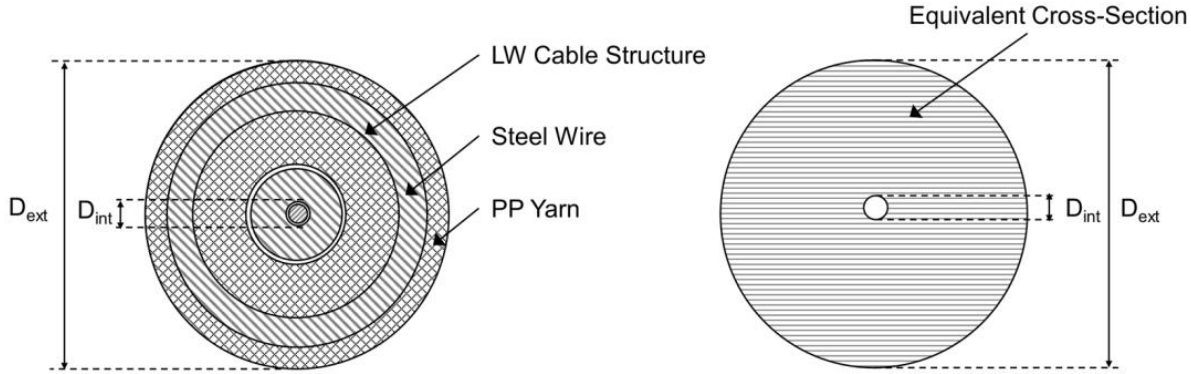

Figure 11. SA submarine cable and its equivalent cross-section.

Since submarine cables are often fully embedded in the seabed due to prevailing sea conditions [32], a burial depth of the cable has been considered equal to 0.5 m, measured from its centerline (H_b = 0.5 m). The cable-soil interaction, which has been simulated with PSI elements, is based on the analytical expressions of ALA guidelines [69], in terms of the peak friction angle, φ_p, which has been set equal to 30°, the coefficient of lateral earth pressure at rest, $K_0 = (1 - \sin\varphi) = 0.5$, as well as reduction factor f, which is taken as equal to 0.6 (smooth polypropylene surface of the cable). The friction between the seabed and the cable has been evaluated considering the effective soil unit weight equal to 5.89 kN/m^3. Figure 12a presents the cable deformations in terms of absolute maximum axial strains at the middle of the cable section for net bedrock displacement equal to 2 cm, 4 cm, 6 cm, 8 cm, 16 cm and 32 cm, for dip angle 60°, whereas Figure 12b displays the actual displacement of the cable.

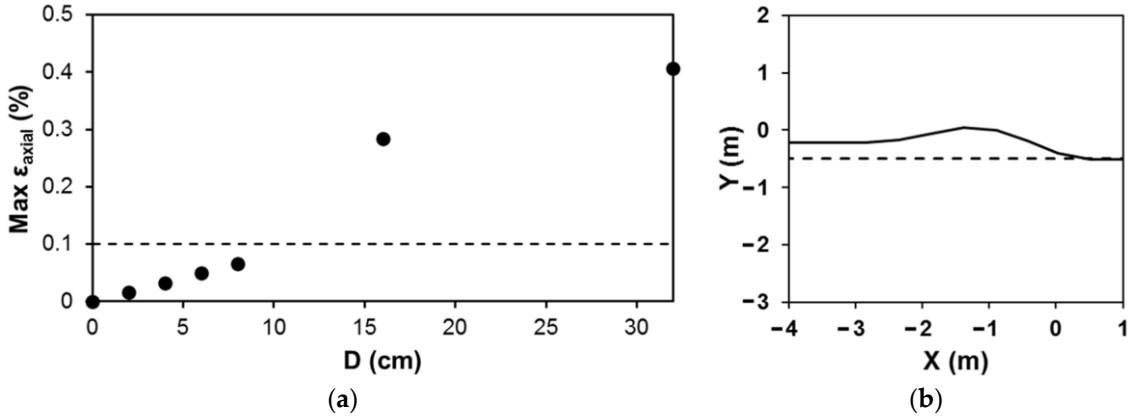

Figure 12. (**a**) Maximum axial strains of the submarine telecommunication cable for different net bedrock displacements, and (**b**) actual displacement of the cable at the fault rupture zone.

3.3. Case Study 2: Submarine Power Cable Connecting Crete with Egypt

The same criteria with Case Study 1 (i.e., seabed inclination, bathymetry, seismically active fault zones) have also been adopted in this application and the five scenarios described in the previous subsection have also been examined in the case of a power transmission cable connecting Crete with Egypt. Table 4 lists the weight values that resulted from the AHP for each of the aforementioned scenarios, as well as the rating score of each sub-criterion. Figure 13a,b present five alternative cost (and length) minimized cable routes. Route I corresponds to the extreme scenario with significantly greater influence to bathymetry, Route II represents the realistic scenario and Route III denotes the extreme scenario with a greater weight value to seismic fault zones. Route IV constitutes the intermediate scenario, whereas Route V refers to the scenario where seabed inclination has extreme influence.

The proposed numerical model for a power cable has been applied to assess the problem of fault-cable intersection. The equivalent and simplified cross-section presented in Figure 5 has been developed. The diameter, D is 64 mm, the equivalent elastic modulus has been set equal to 56 GPa. Similarly to Case Study 1, the cable's burial depth has been set equal to 0.5 m, whereas φ_p, K_0 and f have been set as equal to 30°, 0.5 and 0.6, respectively. The friction between the seabed and the cable has been evaluated considering the effective soil unit weight, which has been set as equal to 5.89 kN/m^3. Figure 14a displays the cable deformations in terms of absolute maximum axial strains at the middle of the cable section for the net bedrock displacement equal to 2 cm, 4 cm, 6 cm and 8 cm, 16 cm and 32 cm, for dip angle 60°, whereas Figure 14b depicts the actual displacement of the cable.

Table 4. Weight-influence and rating score of each of the adopted criteria and sub-criteria for Case Study 2.

Criteria	Weight-Influence (%)					Sub-Criteria	Rating Score
	Scenarios						
	1	2	3	4	5		
Seabed Inclination (°)	82	9	9	33	30	0–10 10–20 20–30 30–40 >40	1 2 3 4 5
Bathymetry (m)	9	82	9	33	7	0–1000 1000–2000 2000–3000 3000–4000 >4000	1 2 3 4 5
Seismic Fault Zones	9	9	82	34	63	Cretan–Rhodes ridge Hellenic trench East Mediterranean ridge Herodotus trough West Cyprus arc South Cyprus trench	5 5 3 - - -

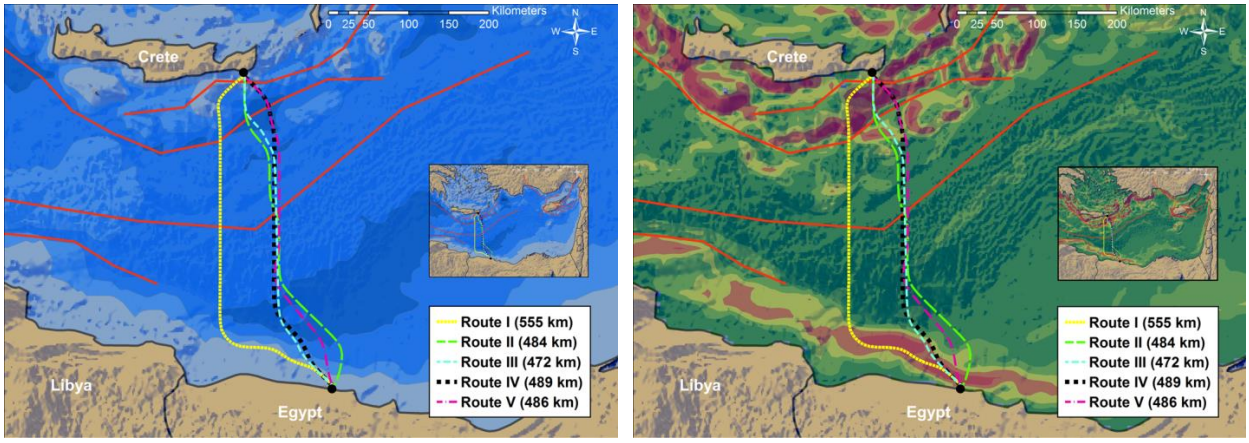

(**a**) (**b**)

Figure 13. Proposed alternative routes and seismically active fault zones: (**a**) with the bathymetry as a background and (**b**) with the seabed inclination as a background.

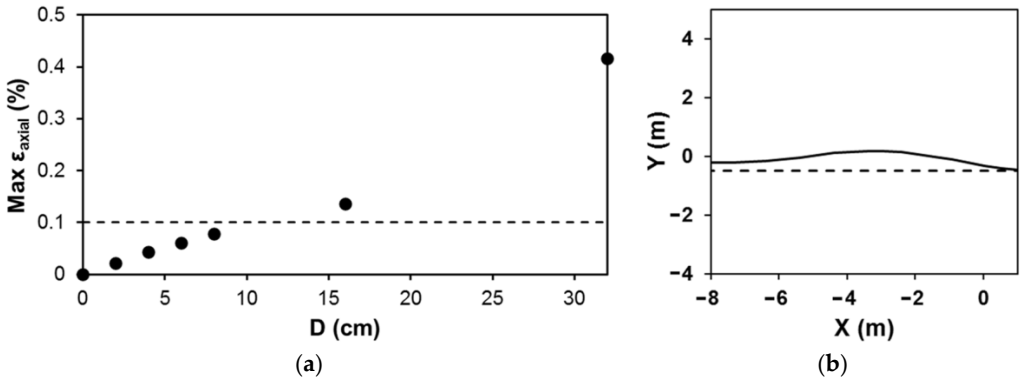

(**a**) (**b**)

Figure 14. (**a**) Maximum axial strains of the submarine power cable for different net bedrock displacements, and (**b**) the actual displacement of the cable at the fault rupture zone.

4. Discussion

Results from Figure 7a reveal that the eastern Mediterranean Sea is characterized by deep and ultra-deep waters, reaching depths of up to 4000 m. Figure 7b illustrates that the central part of the examined area is mostly characterized by a very smooth seabed inclination, whereas steep slopes are located near the coasts of southwestern Greece, southern Crete, Rhodes and Turkey, thus, forming a wide basin. Figure 7c,d demonstrate that the eastern Mediterranean Sea is a seismic-prone and tectonically active region, as intense seismicity, especially near the Cretan coastline, and several fault zones can be easily observed. As a consequence, a CL crossing these areas would be subjected to various offshore earthquake-related geohazards, including seismic fault rupture and potential submarine landslides.

However, at this point it is important to note that local site conditions constitute a critical factor that play a key role in the earthquake-triggered geohazard of seismic fault rupture and the structural response of the crossing CL. On the one hand, the presence of soft sediments that cover the ruptured bedrock might have a beneficial impact on the kinematic distress of the CL, as they tend to absorb the abrupt bedrock displacements, thus leading to a smoother displacement profile at the seabed. On the other hand, an outcropped fault (i.e., without the presence of overlying soft sediments) may have an unfavorable impact on the structural behavior of the CL, as it has been evidenced in the case of onshore pipelines [70].

According to Figure 8, medium-to-thick sediments are located at the central part of the Mediterranean Sea and near the delta of the Nile River in the sea area north of Egypt. Conversely, the areas near the coasts of Crete, Libya, eastern Egypt and Cyprus are characterized by very thin or even none overlying soft sediments. In a previous version of the developed smart tool, Makrakis et al. [43] selected the optimal route of an offshore gas pipeline connecting the island of Crete to Cyprus. The optimal route was crossing the East Mediterranean ridge and the role of sediments, which had been assumed to cover the ridge, was taken into account via an extensive numerical investigation. The consequent structural distress of the crossing CL was assessed and the problem of a pipeline-blind-fault intersection was effectively addressed. The authors revealed that the examined facility could safely cross the East Mediterranean ridge due to the beneficial impact of the overlying seabed sediments.

Herein, the more adverse problem of an outcropped-fault-cable intersection has been examined. The fault zones near the island of Crete (i.e., Cretan–Rhodes ridge, Hellenic trench), the Herodotus trough, as well as the fault zones near Cyprus (i.e., West Cyprus arc, South Cyprus trench) have been assumed to be covered from zero to very thin sediments. Consequently, they have received a greater rating score during the application of the smart decision-support tool, compared to the East Mediterranean ridge, as shown in Tables 3 and 4. It is noted that the Cretan–Rhodes ridge, as well as the seismic fault zones near Cyprus have not been taken into account in Case Study 1 (telecommunication cable between Crete and Libya), whereas Case Study 2 (power cable between Crete and Egypt) has not considered the Herodotus trough and the seismic fault zones near Cyprus. This is due to the fact that the aforementioned fault zones had no effect on the optimal route selection process. Finally, it is important to mention that in engineering practice, minimizing the fault-cable intersection length (i.e., vertical crossing) is expected to reduce the risk of cable structural failures [5].

Apart from the seismically active fault zones, bathymetry and seabed inclination have also been selected as basic criteria for the optimal route selection of the submarine cables. As presented in Tables 3 and 4, the applied rating score is in line with the engineering practice in the field of submarine cable routing. In general, the length (and consequently the cost) of submarine cables is directly related to the depth at which they are laid. However, submarine cables that are laid at shallow depths (up to 300 m) are frequently exposed to the geohazard of slope instability (under static and/or seismic conditions), as almost 30% of cable structural damages are related to seabed slope failure [71]. Apart from the issues

related to structural integrity, a large seabed inclination might considerably increase the cable cost [72]. Hence, a rating score that increases with the increase of bathymetry and seabed inclination has been assigned. It is worth noting that in practice, cables crossing steep seabed slopes are commonly laid perpendicular to the slope in order to reduce their contact surface area with the seabed [24].

Figure 9 illustrates the reliability and effectiveness of the developed decision-support tool. An optimal route has been derived from the application of the smart tool and is compared with the route of a real engineering project, namely the EuroAsia Interconnector. The proposed route is almost identical to the EuroAsia routing, while the differences observed in the central and eastern parts might be attributed to the lack of data (i.e., topographic survey, geotechnical study, etc.) and further information regarding the actual project's routing (i.e., weight values, rating scores, etc.).

Figure 10a,b are related to Case Study 1, i.e., the telecommunication cable connecting Crete to Libya. Route I is based on the realistic scenario and crosses almost vertically the critical fault zones of the Hellenic trench and Herodotus trough, while inevitably passing through the areas characterized by steep slopes (i.e., near the island of Crete and near the coasts of Libya). However, the length (and cost) of Route I is minimized within these potentially dangerous areas (due to vertical crossing). Route II, where seabed inclination has been assigned high weight values, is very close to Route III, where seismic fault zones have been set highly influential. Both Routes II and III cross the critical fault zones with a perpendicular orientation, whereas the latter constitutes the shortest among the proposed alternative routings.

Route IV corresponds to the intermediate scenario and it can be clearly seen that the medium effect of bathymetry has played a key role. Although Route IV has successfully avoided deep and ultra-deep waters, its length is considerably increased and passes through the steep slopes located near the island of Crete. It is noted that the Hellenic trench is crossed at an angle different than 90°. The 457 km-long Route V is dominated by the effect of bathymetry and constitutes the longest route. An extensive part of Route V passes through the steep slopes near Libya and Crete, whereas the critical fault zones are not vertically crossed.

In addition, it can be easily observed that the existing cable route is almost straight, crossing for several kilometers the dangerous zones near the Cretan coastline, and consequently, it is susceptible to the geohazard of earthquake-triggered submarine landslides. Proposed Routes I, II and III differ from the existing cable in the way they pass through the potentially unstable zones, as well as the crossing of the Hellenic trench.

Figure 13a,b refer to Case Study 2, i.e., the power cable connecting the island of Crete to Egypt. Route I, where the weight value of bathymetry has been set equal to 82%, constitutes the longest proposed route (i.e., 555 km long) and differs significantly from the other proposed routings. This is attributed to the fact that deep and ultra-deep waters have been rated higher, compared to shallower depths, and consequently Route I has avoided the deep waters north of Egypt. The low influence of seabed inclination and seismic fault zones has led Route I to pass through an extensive zone of a large seabed inclination (>30°), and cross, at an angle different from 90°, the Cretan–Rhodes ridge and the Hellenic trench.

Route II is a 484 km-long cable routing corresponding to the scenario with realistic weight values (i.e., slopes 30%—bathymetry 7%—seismic fault zones 63%). Seismic fault zones are highly influential, and consequently Route II crosses almost vertically the Cretan–Rhodes ridge and the Hellenic trench. Conversely, the East Mediterranean ridge, which has been assigned a lower rating score, is crossed at an angle different than 90°. Although steep slopes near Egypt are successfully avoided (i.e., crossed vertically for very few kilometers), a notable part of Route II passes through a potentially dangerous high-slope region near the island of Crete. This is due to the impact of the seabed inclination, which is considerably lower than the effect of seismic fault zones. The 472 km-long Route III is the shortest proposed route and it is almost identical to Route II, as they differ only in the way they cross the steep slopes near Egypt. In Route III, the seabed inclination has

been assigned a lower weight value (i.e., 9%), compared to the realistic scenario of Route II. As a consequence, Route III has an inclined orientation within the steep slopes near Egypt.

Similarly, Route IV and V constitute almost identical routings, differences can be observed in the way they cross the steep slopes near Egypt. Route V, in which the seabed inclination is highly influential, crosses almost vertically both the steep slopes near the island of Crete and the potentially dangerous zone near Egypt. Moreover, Route IV, where the seabed inclination has assigned a moderate weight value, is perpendicularly oriented within the steep slopes near the island of Crete, while a large part of the route passes through the steep slopes north of Egypt. This difference is attributed to the considerable influence of bathymetry, as it can be easily seen that a smaller part of Route IV passes through the deep waters near Egypt, compared to Route V. Finally, although both routes have successfully minimized the intersection with the Hellenic trench (i.e., vertical crossing), the crossing angle with the Cretan–Rhodes ridge differs significantly from 90°.

The geomorphology of the examined area is dominated by fault zones that lead to reverse bedrock dislocation of the order of 4 cm per year [73]. Considering that the complete avoidance of the seismically active fault zones is not feasible, and following the engineering practice, the decision-support tool has proposed, among others, cable routings that cross (almost) vertically these critical areas (i.e., for the scenarios where seismic fault zones were assigned great weight values). These routes have been numerically examined against the earthquake-triggered geohazard of fault rupture. It has to be stressed that the problem of reverse fault-cable intersection has not been investigated so far. Conversely, significant research interest has been concentrated on the problem of reverse faut-pipeline intersection, where it has been reported that an almost vertical crossing could lead to early structural failures of CLs even for a very small bedrock dislocation [39]. In the current study, a parametric investigation was carried out considering a net bedrock displacement ranging from 2 cm to 32 cm with a dip angle equal to 60°.

Cables that cross shallow waters are generally armored and buried on the seabed, thus increasing the construction costs. At deep and ultra-deep waters, where the threats from human-made hazards are drastically reduced, designers usually prefer light weight cables [6,24]. However, the tectonic and geomorphological peculiarities of the area under consideration have led the authors to conservatively consider armored cables at both shallow and deep waters and to develop realistic FE models for this type of cable.

Figures 12a and 14a present that the absolute maximum axial strains increase almost linearly for relatively small net bedrock displacements, for both the examined submarine cables (i.e., telecommunication and power cables). However, a non-linear increase can be easily seen for greater displacements. The linear behavior is attributed to the elastic material properties that have been utilized for the numerical analyses. Conversely, the non-linear relationship of the cable deformations for large net fault offsets could be explained considering the non-linearities of the PSI FE. The resulting strains have been compared to an indicative strain limit threshold equal to 0.1%, which has been derived from the studies of Reda et al. [74] and Wang et al. [32]. It can be observed that strains greater than 0.1% have been developed for a bedrock offset of $D \geq 16$ cm, regardless of the type of the cable.

The proposed numerical model can be successfully utilized to investigate the structural response of a submarine cable subjected to the geohazard of fault rupture. In particular, it can be easily observed from Figure 4a,b that the numerical FE model developed from the authors presents a very satisfactory agreement with the numerical models and the full-scale experiment of Wang et al. [32]. Although small discrepancies are observed for relatively low lateral soil displacements, the proposed numerical model tends to be slightly closer to the experimental results, compared to the numerical model that was developed by Wang et al. [32].

Finally, it is important to mention that the multidisciplinary topic of the present study is characterized by several uncertainties that are difficult to be accurately quantified. Undoubtedly, a significant volume of geodata is required for a reliable and accurate representation of the routing analysis criteria. However, the accurate mapping of off-

shore earthquake-triggered geohazards constitutes a demanding geological procedure. Earthquake-triggered geohazards cannot be precisely evaluated, since data related to the topography, geology and geomorphology of the seabed are limited. Such geodata are usually derived from time-consuming geophysical surveys and potentially-inaccurate digitized geological maps of the seabed.

Moreover, the quantitative assessment of offshore earthquake-triggered geohazards and the consequent distress of crossing CLs is characterized by various epistemic and aleatory uncertainties. For instance, seismic fault zones are unrealistically represented within the GIS environment as linear entities, with starting and ending points and specific dimensions without an accurate mapping of critical factors, such as slip potential, path propagation, secondary faults, etc.

5. Conclusions

The current paper presents a smart decision-support tool that can be used for the optimal route selection of submarine cables, since it is capable of assessing whether an examined routing could effectively cross a (seismically) geologically hazardous area. For this purpose, the advanced capabilities of GIS in finding the optimal path between two geographic points are successfully combined with a multi-criteria decision method to transform the qualitative prioritization of the adopted criteria into weight values. In this manner, several cable routes are proposed aiming for length- and cost-minimization. For the routings subjected to tectonic faulting, the problem of fault-cable intersection is quantitatively assessed via realistic numerical models. The resulting cable distress, in terms of strains, is integrated into the GIS model and the optimal route is selected by taking into account the criticality of the problem (i.e., exceedance of the allowable strain limits).

The developed numerical models have been verified against experimental results from the literature, whereas the accuracy of the GIS-based routing analysis has been verified against an under-design power transmission cable connecting Greece to Cyprus. The applicability of the smart decision-support tool is presented in two more realistic case studies in the southeastern Mediterranean Sea related to one telecommunication and another power transmission cable. Five different user-defined scenarios have been examined for these case studies, resulting in five alternative cable routings. The proposed routes differ in length, but also in the way that they cross the seismically active fault zones, the potentially unstable steep slopes, as well as the deep and ultra-deep waters. Regarding the telecommunication cable, a useful comparison with the existing routing has been performed. Nevertheless, it should be stressed that the actual comparison with existing engineering problems is indicative, due to the lack of all of the required data and the resulting simplifications.

The examined real-life case studies have been used mainly to illustrate the applicability and the effectiveness of the proposed tool. Moreover, some useful conclusions can be derived from the specific applications:

- Southeastern Mediterranean Sea is prone to offshore geohazards and especially to tectonic faulting, mainly near the coastline of the island of Crete, Greece. This fact highlights the necessity for a very careful seismic design and optimal route selection of crossing critical lifelines;
- All of the alternative routes inevitably pass through extensive zones of moderate-to-large seabed inclinations due to the characteristics of the examined region. However, the assigned weight values corresponding to the seabed inclination in each scenario affect the orientation of the proposed routes within these zones;
- Very long routings have been derived when bathymetry has been given a high importance;
- Assigning high importance to seismic fault zones leads to the shortest routes, which cross almost vertically the fault zones. Nonetheless, relatively high absolute maximum axial strains for medium net bedrock displacements have been observed, regardless of the cable type (i.e., telecommunication or power transmission). Hence, a more sophisticated design is required for seismic events with a higher return period.

The process of optimal route selection is not a straightforward task in large-scale engineering projects, even for experienced engineers, and it should be examined on a case-by-case basis, taking into account all important parameters. Certainly, optimum route selection via automated decision-support tools can considerably reduce the probability of failure and the life-cycle costs of the examined lifeline, minimizing the impact of human errors and bias. Despite its present capabilities, further improvements of the proposed smart tool are required, focusing on the enrichment of the criteria adopted during the routing analysis, the automatization of the whole process, as well as the adopted optimization methodology.

Author Contributions: Conceptualization, N.M., P.N.P. and Y.T.; methodology, N.M., P.N.P. and Y.T.; software, N.M.; validation, N.M., P.N.P. and Y.T.; formal analysis, N.M. and Y.T.; investigation, N.M., P.N.P. and Y.T.; resources, N.M., P.N.P. and Y.T.; data curation, N.M.; writing—original draft preparation, N.M., P.N.P. and Y.T.; writing—review and editing, N.M., P.N.P. and Y.T.; visualization, N.M., P.N.P. and Y.T.; supervision, Y.T.; project administration, Y.T. All authors have read and agreed to the published version of the manuscript.

Funding: The research work was supported by the Hellenic Foundation for Research and Innovation (HFRI) under the 4th Call for HFRI Ph.D. Fellowships (Fellowship Number: 9408). This support is gratefully acknowledged by the first author.

Institutional Review Board Statement: Not applicable.

Informed Consent Statement: Not applicable.

Data Availability Statement: Not applicable.

Conflicts of Interest: The authors declare no conflict of interest.

References

1. Wang, W.; Yan, X.; Li, S.; Zhang, L.; Ouyang, J.; Ni, X. Failure of Submarine Cables Used in High-Voltage Power Transmission: Characteristics, Mechanisms, Key Issues and Prospects. *IET Gener. Transm. Distrib.* **2021**, *15*, 1387–1402. [CrossRef]
2. Wang, Q.; Guo, J.; Wang, Z.; Tahchi, E.; Wang, X.; Moran, B.; Zukerman, M. Cost-Effective Path Planning for Submarine Cable Network Extension. *IEEE Access* **2019**, *7*, 61883–61895. [CrossRef]
3. Msongaleli, D.L.; Dikbiyik, F.; Zukerman, M.; Mukherjee, B. Disaster-Aware Submarine Fiber-Optic Cable Deployment for Mesh Networks. *J. Light. Technol.* **2016**, *34*, 4293–4303. [CrossRef]
4. Taormina, B.; Bald, J.; Want, A.; Thouzeau, G.; Lejart, M.; Desroy, N.; Carlier, A. A Review of Potential Impacts of Submarine Power Cables on the Marine Environment: Knowledge Gaps, Recommendations and Future Directions. *Renew. Sustain. Energy Rev.* **2018**, *96*, 380–391. [CrossRef]
5. Zhao, M.; Chow, T.W.S.; Tang, P.; Wang, Z.; Guo, J.; Zukerman, M. Route Selection for Cabling Considering Cost Minimization and Earthquake Survivability via a Semi-Supervised Probabilistic Model. *IEEE Trans. Ind. Informa.* **2017**, *13*, 502–511. [CrossRef]
6. Burnett, D.R.; Beckman, R.; Davenport, T.M. *Submarine Cables: The Handbook of Law and Policy*; Burnett, D.R., Beckman, R., Davenport, T.M., Eds.; Martinus Nijhoff: Leiden, The Netherlands, 2013; ISBN 978-90-04-26033-7.
7. Wang, X.; Wang, Z.; Tahchi, E.; Zukerman, M. Submarine Cable Path Planning Based on Weight Selection of Design Considerations. *IEEE Access* **2021**, *9*, 123847–123860. [CrossRef]
8. Hong, C.; Estefen, S.F.; Lourenço, M.I.; Wang, Y. A Nonlinear Constrained Optimization Model for Subsea Pipe Route Selection On an Undulating Seabed with Multiple Obstacles. *Ocean Eng.* **2019**, *186*, 106088. [CrossRef]
9. Ganganath, N.; Cheng, C.T.; Tse, C.K. A Constraint-Aware Heuristic Path Planner for Finding Energy-Efficient Paths on Uneven Terrains. *IEEE Trans. Ind. Informa.* **2015**, *11*, 601–611. [CrossRef]
10. Warntz, W. Transportation, Social Physics, And The Law Of Refraction. *Prof. Geogr.* **1957**, *9*, 2–7. [CrossRef]
11. Marinoni, O. Implementation of the Analytical Hierarchy Process with VBA in ArcGIS. *Comput. Geosci.* **2004**, *30*, 637–646. [CrossRef]
12. Aly, M.H.; Giardino, J.R.; Klein, A.G. Suitability Assessment for New Minia City, Egypt: A GIS Approach to Engineering Geology. *Environ. Eng. Geosci.* **2005**, *11*, 259–269. [CrossRef]
13. Youssef, A.M.; Pradhan, B.; Tarabees, E. Integrated Evaluation of Urban Development Suitability Based on Remote Sensing and GIS Techniques: Contribution from the Analytic Hierarchy Process. *Arab. J. Geosci.* **2011**, *4*, 463–473. [CrossRef]
14. Uy, P.D.; Nakagoshi, N. Application of Land Suitability Analysis and Landscape Ecology to Urban Greenspace Planning in Hanoi, Vietnam. *Urban For. Urban Green.* **2008**, *7*, 25–40. [CrossRef]

15. Yildirim, V.; Yomralioglu, T.; Nisanci, R.; Erbas, Y.S.; Bediroglu, S. Natural Gas Transmission Pipeline Route Selection Using GIS and AHP. In Proceedings of the 6th International Pipeline Technology Conference, Ostend, Belgium, 6–9 October 2013.
16. Wan, J.; Qi, G.; Zeng, Z.; Sun, S. The Application of AHP in Oil and Gas Pipeline Route Selection. In Proceedings of the 19th International Conference on Geoinformatics, Shanghai, China, 24–26 June 2011.
17. Atkinson, D.M.; Deadman, P.; Dudycha, D.; Traynor, S. Multi-Criteria Evaluation and Least Cost Path Analysis for an Arctic All-Weather Road. *Appl. Geogr.* **2005**, *25*, 287–307. [CrossRef]
18. King, T.; Phillips, R.; Johansen, C. Pipeline Routing and Burial Depth Analysis Using GIS Software. In Proceedings of the Society of Petroleum Engineers—Arctic Technology Conference, Houston, TX, USA, 7–9 February 2011; pp. 445–455.
19. Haneberg, W.C.; Bruce, B.; Drazba, M.C. Using Qualitative Slope Hazard Maps and Quantitative Probabilistic Slope Stability Models to Constrain Least-Cost Pipeline Route Optimization. In Proceedings of the Offshore Technology Conference, Houston, TX, USA, 6–9 May 2013; pp. 1–11.
20. Devine, C.A.; Haneberg, W.C.; Lee, H.; Liu, M.L.; Chang, G.A. A Sensible Approach to Subsea Pipeline Route Determination—Moving from Hand-Drawn Routes to Geologically-Constrained, Least-Cost Optimized Paths. *Proc. Annu. Offshore Technol. Conf.* **2016**, *1*, 872–888. [CrossRef]
21. Balogun, A.L.; Matori, A.N.; Hamid-Mosaku, A.I.; Umar Lawal, D.; Ahmed Chandio, I. Fuzzy MCDM-Based GIS Model for Subsea Oil Pipeline Route Optimization: An Integrated Approach. *Mar. Georesources Geotechnol.* **2017**, *35*, 961–969. [CrossRef]
22. American Bureau of Shipping. *Guidance Notes on Subsea Pipeline Route Determination*; American Bureau of Shipping: Houston, TX, USA, 2016.
23. Randolph, M.; Gourvenec, S. *Offshore Geotechnical Engineering*, 2nd ed.; CRC Press: London, UK, 2011; ISBN 9781351988919.
24. Carter, L.; Burnett, D.; Drew, S.; Marle, G.; Hagadorn, L.; Bartlett-McNeil, D.; Irvine, N. *Submarine Cables and the Oceans—Connecting the World*; UNEP-WCMC Report: Cambridge, UK, 2009.
25. Berger, A.; Kousky, C.; Zeckhauser, R. Obstacles to Clear Thinking about Natural Disasters: Five Lessons for Policy. In *Risking House and Home: Disasters, Cities, Public Policy*; Quigley, J.M., Rosenthal, L.A., Eds.; Berkeley Public Policy Press: Berkeley, CA, USA, 2008; pp. 73–94.
26. Makrakis, N.; Psarropoulos, P.N.; Chatzidakis, D.; Tsompanakis, Y. Optimal Route Selection of Offshore Pipelines Subjected to Submarine Landslide. *Open Civ. Eng. J.* **2022**, *16*, e187414952209160. [CrossRef]
27. Hsu, S.-K.; Kuo, J.; Lo, C.-L.; Tsai, C.-H.; Doo, W.-B.; Ku, C.-Y.; Sibuet, J.-C. Turbidity Currents, Submarine Landslides and the 2006 Pingtung Earthquake off SW Taiwan. *Terr. Atmos. Ocean. Sci.* **2008**, *19*, 767–772. [CrossRef]
28. Kobayashi, M. Experience of Infrastructure Damage Caused by the Great East Japan Earthquake and Countermeasures Against Future Disasters. *IEEE Commun. Mag.* **2014**, *52*, 23–29. [CrossRef]
29. Tran, P.N.; Saito, H. Geographical Route Design of Physical Networks Using Earthquake Risk Information. *IEEE Commun. Mag.* **2016**, *54*, 131–137. [CrossRef]
30. Agrawal, A.; Bhatia, V.; Prakash, S. Network and Risk Modeling for Disaster Survivability Analysis of Backbone Optical Communication Networks. *J. Light. Technol.* **2019**, *37*, 2352–2362. [CrossRef]
31. Wang, Z.; Wang, Q.; Zukerman, M.; Guo, J.; Wang, Y.; Wang, G.; Yang, J.; Moran, B. Multiobjective Path Optimization for Critical Infrastructure Links with Consideration to Seismic Resilience. *Comput. Civ. Infrastruct. Eng.* **2017**, *32*, 836–855. [CrossRef]
32. Wang, Y.; Fu, C.; Qin, X. Numerical and Physical Modeling of Submarine Telecommunication Cables Subjected to Abrupt Lateral Seabed Movements. *Mar. Georesources Geotechnol.* **2020**, *39*, 1307–1319. [CrossRef]
33. Cao, C.; Wang, Z.; Zukerman, M.; Manton, J.H.; Bensoussan, A.; Wang, Y. Optimal Cable Laying Across an Earthquake Fault Line Considering Elliptical Failures. *IEEE Trans. Reliab.* **2016**, *65*, 1536–1550. [CrossRef]
34. Jalali, H.H.; Rofooei, F.R.; Khajeh, A.A.N. Performance of Buried Gas Distribution Pipelines Subjected to Reverse Fault Movement. *J. Earthq. Eng.* **2018**, *22*, 1068–1091. [CrossRef]
35. Saiyar, M.; Ni, P.; Take, W.A.; Moore, I.D. Response of Pipelines of Differing Flexural Stiffness to Normal Faulting. *Geotechnique* **2016**, *66*, 275–286. [CrossRef]
36. Tsatsis, A.; Loli, M.; Gazetas, G. Pipeline in Dense Sand Subjected to Tectonic Deformation from Normal or Reverse Faulting. *Soil Dyn. Earthq. Eng.* **2019**, *127*, 105780. [CrossRef]
37. Fadaee, M.; Farzaneganpour, F.; Anastasopoulos, I. Response of Buried Pipeline Subjected to Reverse Faulting. *Soil Dyn. Earthq. Eng.* **2020**, *132*, 106090. [CrossRef]
38. Triantafyllaki, A.; Papanastasiou, P.; Loukidis, D. Numerical Analysis of the Structural Response of Unburied Offshore Pipelines Crossing Active Normal and Reverse Faults. *Soil Dyn. Earthq. Eng.* **2020**, *137*, 106296. [CrossRef]
39. Joshi, S.; Prashant, A.; Deb, A.; Jain, S.K. Analysis of Buried Pipelines Subjected to Reverse Fault Motion. *Soil Dyn. Earthq. Eng.* **2011**, *31*, 930–940. [CrossRef]
40. Karamitros, D.K.; Bouckovalas, G.D.; Kouretzis, G.P. Stress Analysis of Buried Steel Pipelines at Strike-Slip Fault Crossings. *Soil Dyn. Earthq. Eng.* **2007**, *27*, 200–211. [CrossRef]
41. Karamitros, D.K.; Bouckovalas, G.D.; Kouretzis, G.P.; Gkesouli, V. An Analytical Method for Strength Verification of Buried Steel Pipelines at Normal Fault Crossings. *Soil Dyn. Earthq. Eng.* **2011**, *31*, 1452–1464. [CrossRef]

42. Liu, X.; Zhang, H.; Wu, K.; Xia, M.; Zheng, Q.; Li, Y.; Ndubuaku, O.; Adeeb, S. A Refined Analytical Strain Analysis Method for Offshore Pipeline under Strike-Slip Fault Movement Considering Strain Hardening Effect of Steel. *Ships Offshore Struct.* **2020**, *15*, 215–226. [CrossRef]
43. Makrakis, N.; Psarropoulos, P.; Chatzidakis, D.; Tsompanakis, Y. Route Optimization of Offshore Lifelines Taking Into Account Potential Earthquake-Related Geohazards. *Front. Built Environ.* **2020**, *6*, 112. [CrossRef]
44. ESRI (Environmental Systems Resource Institute). *ArcGIS Desktop, Release 10.4*; ESRI: Redlands, CA, USA, 2016.
45. Effat, H.A.; Hassan, O.A. Designing and Evaluation of Three Alternatives Highway Routes Using the Analytical Hierarchy Process and the Least-Cost Path Analysis, Application in Sinai Peninsula, Egypt. *Egypt. J. Remote Sens. Space Sci.* **2013**, *16*, 141–151. [CrossRef]
46. Saaty, T.L. Decision Making—The Analytic Hierarchy and Network Processes (AHP/ANP). *J. Syst. Sci. Syst. Eng.* **2004**, *13*, 1–35. [CrossRef]
47. Saaty, T.L. A Scaling Method for Priorities in Hierarchical Structures. *J. Math. Psychol.* **1977**, *15*, 234–281. [CrossRef]
48. Chuang, P.T. Combining the Analytic Hierarchy Process and Quality Function Deployment for a Location Decision from a Requirement Perspective. *Int. J. Adv. Manuf. Technol.* **2001**, *18*, 842–849. [CrossRef]
49. Saaty, T.L. Decision Making with the Analytic Hierarchy Process. *Int. J. Serv. Sci.* **2008**, *1*, 83–98. [CrossRef]
50. Chandio, I.A.; Matori, A.N.B.; WanYusof, K.B.; Talpur, M.A.H.; Balogun, A.L.; Lawal, D.U. GIS-Based Analytic Hierarchy Process as a Multicriteria Decision Analysis Instrument: A Review. *Arab. J. Geosci.* **2013**, *6*, 3059–3066. [CrossRef]
51. Bodin, L.; Gass, S.I. On Teaching the Analytic Hierarchy Process. *Comput. Oper. Res.* **2003**, *30*, 1487–1497. [CrossRef]
52. Dijkstra, E.W. A Note on Two Problems in Connexion with Graphs. *Numer. Math.* **1959**, *1*, 269–271. [CrossRef]
53. Stefanakis, E.; Kavouras, M. On the Determination of the Optimum Path in Space. In *Spatial Information Theory A Theoretical Basis for GIS. COSIT 1995*; Frank, A.U., Kuhn, W., Eds.; Lecture Notes in Computer Science; Springer: Berlin/Heidelberg, Germany, 1995; Volume 988, pp. 241–257. [CrossRef]
54. Kang, J.Y.; Lee, B.S. Optimisation of Pipeline route in the Presence of Obstacles Based on a Least Cost Path Algorithm and Laplacian Smoothing. *Int. J. Nav. Archit. Ocean Eng.* **2017**, *9*, 492–498. [CrossRef]
55. Douglas, D.H. Least-Cost Path in GIS Using an Accumulated Cost Surface and Slopelines. *Cartographica* **1994**, *31*, 37–51. [CrossRef]
56. Lee, J.; Stucky, D. On Applying Viewshed Analysis for Determining Least-Cost Paths on Digital Elevation Models. *Int. J. Geogr. Inf. Sci.* **1998**, *12*, 891–905. [CrossRef]
57. Dassault Systèmes Simulia. *Abaqus 6.14 Anal. User's Guide*; Dassault Systèmes Simulia Corp.: Providence, RI, USA, 2014.
58. Makrakis, N.; Psarropoulos, P.N.; Sextos, A.; Tsompanakis, Y. Quantifying the Impact of Soft Surface Soil Layers on Fault Rupture Propagation and Kinematic Distress of Offshore and Onshore Pipelines. In Proceedings of the 17th International Pipeline Technology Conference (PTC), Berlin, Germany, 7–10 March 2022.
59. Fang, P.; Jiang, X.; Hopman, H.; Bai, Y. Mechanical Responses of Submarine Power Cables Subject to Axisymmetric Loadings. *Ocean Eng.* **2021**, *239*, 109847. [CrossRef]
60. Hsieh, M.-C.; Chen, B.-F.; Wang, Y.; Chang, H.-C.; Liu, W.-H.; Hsu, H.-L. Determining Optimal Number of Cores in a Submarine Power Cable. *Int. J. Nav. Archit. Ocean Eng.* **2022**, *14*, 100463. [CrossRef]
61. Ryan, W.B.F.; Carbotte, S.M.; Coplan, J.O.; O'Hara, S.; Melkonian, A.; Arko, R.; Weissel, R.A.; Ferrini, V.; Goodwillie, A.; Nitsche, F.; et al. Global multi-resolution topography synthesis. *Geochem. Geophys. Geosyst.* **2009**, *10*. [CrossRef]
62. Flanders Marine Institute IHO Sea Areas, Version 3. Available online: https://www.marineregions.org/download_file.php?name=World_Seas_IHO_v3.zip (accessed on 15 December 2019).
63. Becker, J.J.; Sandwell, D.T.; Smith, W.H.F.; Braud, J.; Binder, B.; Depner, J.; Fabre, D.; Factor, J.; Ingalls, S.; Kim, S.H.; et al. Global Bathymetry and Elevation Data at 30 Arc Seconds Resolution: SRTM30_PLUS. *Mar. Geod.* **2009**, *34*, 355–371. [CrossRef]
64. USGS United States Geological Survey (USGS). Available online: https://www.usgs.gov/ (accessed on 28 October 2020).
65. IHO-IOC GEBCO Gazetteer of Undersea Feature Names. Available online: https://www.gebco.net/data_and_products/undersea_feature_names/ (accessed on 20 December 2019).
66. Styron, R.; Pagani, M. The GEM Global Active Faults Database. *Earthq. Spectra* **2020**, *36*, 160–180. [CrossRef]
67. Gennesseaux, M.; Winnock, E. Thickness of Mediterranean Plio-Quaternary Sediment. International Hydrographic Organization Data Center for Digital Bathymetry (IHO-DCDB), Nippon Foundation-GEBCO Seabed 2030 Project. Available online: https://www.ngdc.noaa.gov/mgg/ibcm/ibcmsedt.html (accessed on 5 January 2019).
68. EuroAsia Interconnector Route. Available online: https://euroasia-interconnector.com/at-glance/the-route/ (accessed on 3 December 2022).
69. American Lifelines Alliance. *Guidelines for the Design of Buried Steel Pipe*; American Society of Civil Engineers: Reston, VA, USA, 2001.
70. Makrakis, N.; Psarropoulos, P.N.; Tsompanakis, Y. ANN-Based Assessment of Soft Surface Soil Layers' Impact on Fault Rupture Propagation and Kinematic Distress of Gas Pipelines. *Infrastructures* **2023**, *8*, 6. [CrossRef]
71. Kordahi, M.E.; Stix, R.K.; Rapp, R.J.; Sheridan, S.; Lucas, G.; Wilson, S.; Perratt, B. Global Trends in Submarine Cable Systems Faults. In Proceedings of the SubOptic, Dubai, United Arab Emirates, 18–21 April 2016.

72. Huang, S.-W.; Chen, E.; Guo, J. Efficient Seafloor Classification and Submarine Cable Route Design Using an Autonomous Underwater Vehicle. *IEEE J. Ocean. Eng.* **2018**, *43*, 7–18. [CrossRef]
73. Apel, E.V.; Bürgmann, R.; Serpelloni, E. Rigid Block Motion, Interseismic Strain, and Backarc Deformation in the Aegean. In Proceedings of the AGU Fall Meeting Abstracts, San Francisco, CA, USA, 9–14 December 2007.
74. Reda, A.M.; Forbes, G.L.; Al-Mahmoud, F.; Howard, I.M.; McKee, K.K.; Sultan, I.A. Compression Limit State of HVAC Submarine Cables. *Appl. Ocean Res.* **2016**, *56*, 12–34. [CrossRef]